J MATER SCI 41 (2006) 3263–3269

One-step synthetic route for producing nanoslabs: Zn-oriented polycrystalline and single-crystalline zinc oxide

MD. HABIB ULLAH, IL KIM, CHANG-SIK HA*
National Research Laboratory of Nano-Information Materials, Department of Polymer Science & Engineering, Pusan National University, Pusan 609-735, South Korea
E-mail: csha@pusan.ac.kr

Published online: 12 April 2006

In contrast to the present advances in shape control, we report Zn-oriented polycrystalline and single-crystalline ZnO nanoslabs through a facile one-step synthetic route, termed as "sol-gel-via-condensation-gradient" method. The nanoslabs were prepared in aqueous media at low temperature without the use of any surfactant or stabilizing agent. The novel nanoslabs are prepared with large quantity without aggregation. For the polycrystalline nanoslabs, consisting mainly of binary phases $Zn(OH)_2 \cdot 0.5H_2O$ and ZnO, their aspect ratios (length-to-width and width-to-thickness ratios) fall in the approximate range from 2 to 5. Room temperature photoluminescence emissions of the nanoslabs suggest that they are suitable for applications in optoelectronic devices. Especially, the enhanced emission by polycrystalline nanoslabs over single crystal nanoslabs is remarkable. Single-crystalline ZnO nanoslabs exhibited a strong and selective chemical sensitivity toward 4-triethoxysilylaniline.

1. Introduction

Among the semiconducting materials formed from elements in groups II–VI, zinc oxide possesses relative advantages because of the broad range of its high-technology applications. The excellent optical properties of zinc oxide make it suitable for use in photoluminescence devices [1–3] electrodes in solar cells [4–5] and flat-panel displays [6]. Zinc oxide nanostructures can be used as photocatalysts [7], in chemical and biological sensing [8–9] and for energy conversion and storage [10]. Recently, nano-scale single-crystalline zinc oxide has attracted much attention from nano-materials technologists and crystallographers because its properties are expected to depend not only on the structure but also on its shapes, sizes and distributions of sizes (e.g., nanorods and nanowires [3, 11], nanoneedles [12], nanobelts [13], tetrapods [14], and nanotubes [15]). Recently, Tian *et al*. [16] reported the preparation of plate-like ZnO nanostructure, from ZnO nanoparticle precursors in the presence of sodium citrate and hexamethyltetramine. Although 1D semiconductor nanostructures have attracted much attention because of their potential applications in optoelectronic devices, such structures require a greater threshold energy for emission than that required for 2D or 3D nanostructures because of an attenuation of energy in their cavities arising from Fabry–Perot oscillations [17]. In contrast, for nanostructures having slab-like shapes control over the internal architectures of the lattice sites remains a significant challenge, especially when activating them at low energy.

In this paper, we report the preparations of Zn –oriented nanostructures, consisting mainly of binary phases (we refer to them as "polycrystalline nanoslabs"), and single-crystalline ZnO nanoslabs, which have a Wurtzite crystal structure.

Our procedure for preparing the nanoslabs is a very simple, novel, one-step synthesis that occurs at low temperature without the addition of any surfactant or stabilizing agent; we term this approach a "condensation-gradient" method without using any external (e.g., water-cooled) refluxing apparatus (Fig. 1). Our novel approach differs from previous ones methodologically and conceptually in that we control morphological feature and crystal growth without surfactant. Traditional sol-gel methods can be used to grow cluster-type colloid ZnO crystals [18], but it remains a challenge to use these method for shape control. Moreover, hydrothermal methods require

*Author to whom all correspondence should be addressed.
0022-2461
DOI: 10.1007/s10853-005-5474-y

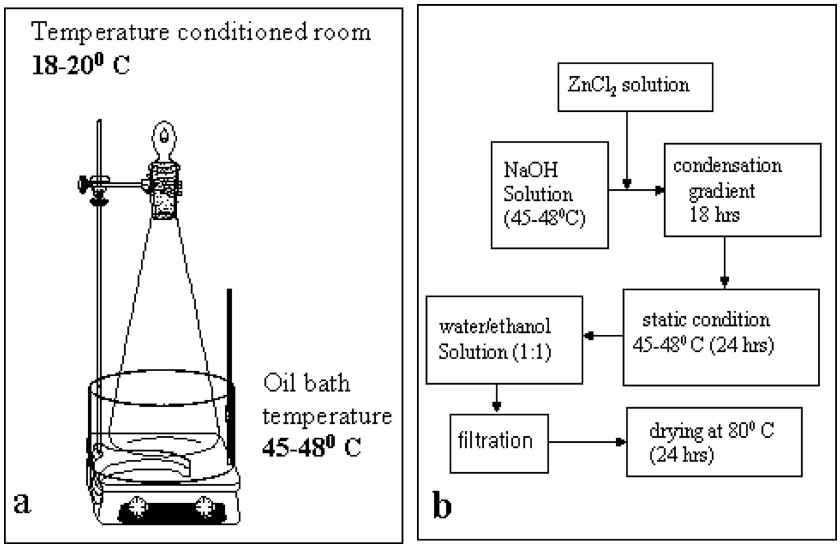

Figure 1 (a) Schematic diagram for the synthetic apparatus used in the "condensation gradient" method; (b) flow chart of the synthetic steps.

high temperatures and the use of special apparatus [19, 20]. The advantage of our "sol-gel-via-condensation-gradient" method over a "sol-gel only" method (i.e., using a sol-gel method at low temperature) is evidenced by the successful growth of high-purity zinc oxide single crystal nanoslabs as well as polycrystalline nanoslabs without any aggregation. As the reactant, we used particular ratios of Zinc chloride (the filler) and sodium hydroxide pellets (the oxygen source) with respect to a critical amount of purified water (the solvent). Sodium hydroxide was used as the growth controller because it provides a rate of crystal growth that is intermediate between those of KOH (too fast) and LiOH (too slow) [19].

2. Experimental details

2.1. Synthesis of polycrystalline nanoslabs

In a typical synthesis, sodium hydroxide pellets (1.0 g, 25 mmol; Shinyo Pure Chemicals Co., Ltd., Osaka, Japan) and distilled water (50 g) were placed into a 100ml Pyrex conical flask. The flask containing the solution was placed in an oil bath (maintained at 45–48°C) and then stirred vigorously with a magnetic bar for 1 h under closed condition so that the temperature of the solution reached that of the bath. A solution of zinc chloride (2.5 g, 18.34 mmol; Yakuri Pure Chemicals Co., Ltd., Osaka, Japan) in deionized water (30 g) was added to the warm (45–48°C) sodium hydroxide solution with constant stirring. The transparent solution changed to an opaque white colloidal suspension. While retaining the conditions (stirring at 45–48°C in the oil bath), the flask was sealed again and the whole system (the sealed flask in the oil bath) was placed in an experimental chamber (temperature conditioned room) maintained at a temperature of 18–20°C. [We call this system a "condensation gradient" because the water that evaporates from the aqueous suspension condenses in the absence of any other (e.g., water-cooled) refluxing apparatus. The upper portion of the closed flask is exposed to the cooler temperature of the chamber even though the suspension in the lower portion remains at 45–48°C under constant stirring.] The condensation gradient conditions were maintained for 18 h; the flask was then placed in another chamber maintained under static conditions (i.e., without stirring) at a temperature of 45–48°C for 24 h. A large amount of white precipitate was obtained; it was dispersed in a water/ethanol solution (1:1) to remove any byproducts. The dispersed product was filtered and dried for 24 h at 80°C.

2.2. Synthesis of single-crystalline nanoslabs

The single-crystalline ZnO nanoslabs were synthesized exactly the same way, but the mass of sodium hydroxide pellets was increased (1.9 g, 47 mmol); all other parameters remained the same.

2.3. Characterization

Powder X-ray diffraction data were collected on a Rigaku Minifex X-ray diffractometer operating at 40 kV and 30 mA using Cu K_α ($\lambda = 1.5401$ Å) radiation. The scan speed was 1°/min in the 2θ range from 1.5 to 75°. The morphologies and size distributions were characterized by using a Hitachi S-4200 field-emission scanning electron microscope (FE-SEM) operating at 5 keV. The TEM and HRTEM studies were performed using a JEOL 2010 electron microscope operating at 200 kV. The energy dispersive spectroscopy (EDS) data were collected on an Oxford LINK ISIS energy dispersive spectrometer attached to the TEM. Before performing the TEM, HRTEM and EDS analyses, the powder samples were dispersed in chloroform and sonicated for 3 h. UV–Vis absorption spectra were measured within the region 200–800 nm using a Hitachi U-2010 spectrophotometer. PL spectra were measured using an ORIEL MS 257 spectrometer; as an excitation source, we used a UV lump (VL-6.LC, VILBER LOURMAT; $\lambda = 365$ nm) placed at an angle of 45°

with respect to the sample container (quartz cuvette with a path length of 1 cm.) TGA data were collected with a Perkin Elmer, TGA 7.

3. Results and discussion

We found that rate of crystal growth, and the resulting shape and size, depend strongly on the amount of NaOH used; i.e., upon the reaction's stoichiometry. This result is consistent with those reported by Spanhel *et al*. [18]. At NaOH concentrations above the reaction stoichiometry, the crystals' structures are unchanged, but their shapes and sizes are influenced by the concentration. Single-crystal nanoslabs were obtained when NaOH concentrations in the matrix solution were higher than the stoichiometric amount, while polycrystalline nanoslabs were obtained when the concentrations were below the stoichiometry of the reactant elements. Various syntheses have been carried out by changing other parameters such as temperature, stirring time, static condition time, and with and without implying the condensation-gradient technique. In this paper, however, we have provided only the data of the resulting products synthesized by the optimal conditions.

Scheme 1 illustrates the basic mechanism of ZnO crystallization when an aqueous $ZnCl_2$ solution is added to an aqueous NaOH solution.

According to Demianets *et al*. [19], a higher concentration of OH^- ions in the solution results in a higher concentration of ZnO_2^{2-} ions and these ZnO_2^{2-} ions are responsible for the polar growth of ZnO crystals.

Fig. 2a indicates that the as-synthesized product obtained using 0.5 M NaOH is highly crystalline. Most of the peaks in the XRD pattern in Fig. 2a correspond well to $Zn(OH)_2{\cdot}0.5H_2O$ and ZnO phases (JCPDS card nos. 20-1436 and 21-1486, respectively). The more-intense peak at $2\theta = 10.91^\circ$ is due to the former phase. This finding may indicate that a greater amount of the $Zn(OH)_2{\cdot}0.5H_2O$ phase, relative to the ZnO phase, exists in the product. This major phase arises as a result of the higher coordinating ability of Zn^{2+} ions at the absence of a sufficient concentration of free OH^- ions in the solution. Fig. 2b displays the XRD pattern of the as-synthesized product obtained at the NaOH concentration of 0.95 M (i.e., above the stoichiometric concentration). This material has the pure hexagonal phase of the Wurtzite structure (space group: $p6_3$ mc) of ZnO (calculated cell constants: a = 3.248 Å, c = 5.208 Å; JCPDS card no. 36-1451). The strong and sharp peaks indicate that this as-synthesized product is highly crystalline and pure. No impurities were detected in this XRD pattern.

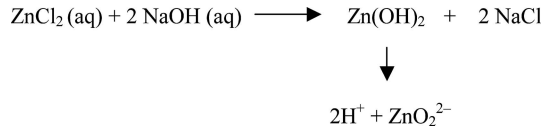

Scheme 1 Basic mechanism of ZnO crystallization

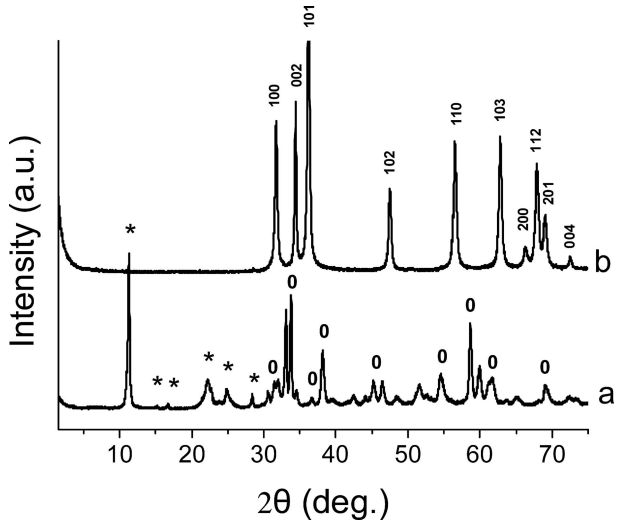

Figure 2 XRD patterns of the as-prepared nanoslabs : (a) polycrystalline material (obtained using 0.5 M NaOH) containing Zn(OH)2·0.5H2O (JCPDS card no. 20-1436) and ZnO (JCPDS card no. 21-1486) phases (labelled with the symbols ∗ and 0, respectively); (b) single-crystalline ZnO (JCPDS card no. 36-1451) having a Wurtzite structure (obtained using 0.95 M NaOH).

Figs 3a and b are typical SEM images of the polycrystalline product obtained using 0.5 M NaOH, at low and high magnifications, respectively. These SEM images reveal that the crystalline product consists mainly of two types of nanoslabs: one has uniform thickness and the other is swelled. The latter type of nanoslabs might grow as a result of the major presence of the $Zn(OH)_2{\cdot}0.5H_2O$ phase. The overall lengths, widths and thicknesses of the nanoslabs lie in the ranges 200–700, 150–300 and 30–60 nm, respectively. By considering the average dimensions of the nanoslabs, their aspect ratios (length-to-width and width-to-thickness ratios) fall in the approximate range from 2 to 5. Low- and high-magnification SEM images (Figs 3c and d) of the single-crystalline ZnO indicate randomly oriented bar-like nanoslabs that have different size distributions relative to those of the polycrystalline nanoslabs. In the SEM images, dendrite-like nanoslabs are also observed.

A typical TEM image of the single-crystalline ZnO nanostructures reveals that dendrite nanoslabs (right-hand inset of Fig. 4a) are also present in addition to the bar-like single nanoslabs as we observed in the SEM image. The top-left image in Fig. 4a presents the ⟨100⟩ zone axis selected area electron diffraction (SAED) pattern (the arrow marks the region from which the SAED pattern was recorded). The single-crystal SAED pattern suggests that the ZnO nanoslabs have hexagonal structures and, with respect to focus of zone axis ⟨100⟩, these nanoslabs grow along the [001] direction. The high-resolution TEM (HRTEM) image is presented in Fig. 4b (the inset marks the magnified image recorded along the ⟨010⟩ zone axis). A clearer view of the magnified image (Fig. 4c) reveals crystal growth along the [101] direction and a lattice spacing (2.49 Å) that corresponds to the (101) planes of the

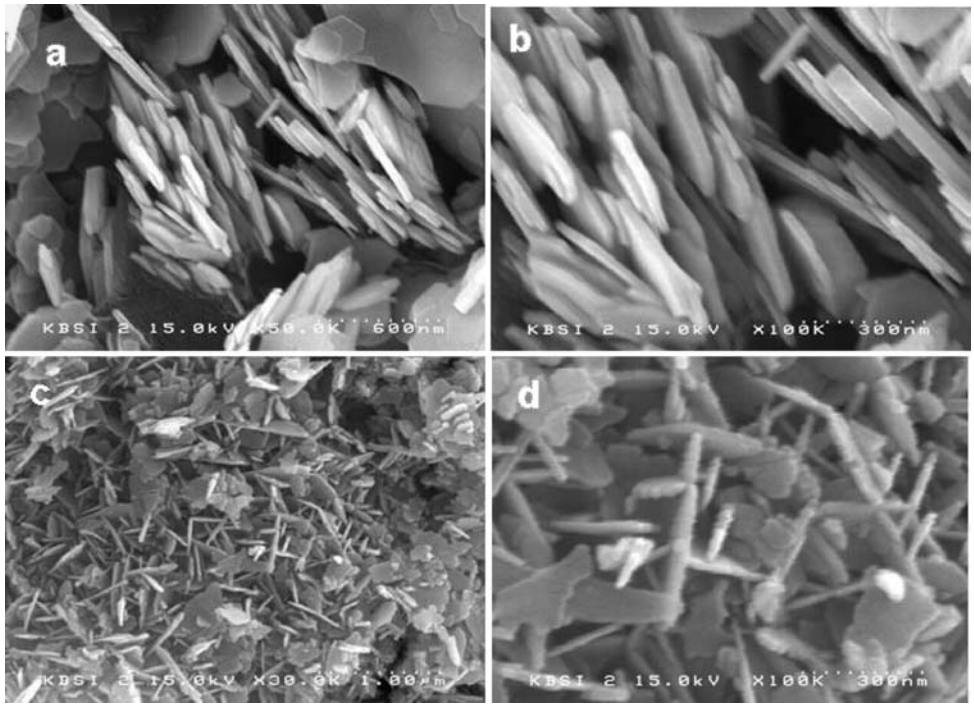

Figure 3 SEM images of the Zn-oriented polycrystalline nanoslabs and single-crystalline ZnO bar-like nanoslabs; (a,b) low- and high-magnification SEM images, respectively, of the polycrystalline nanoslabs, which display swelled nanoslabs beside uniform thickness nanoslabs; (c,d) low- and high magnification SEM images, respectively, of the single-crystalline nanoslabs. In addition, dendritelike nanoslabs are also present in these latter two images.

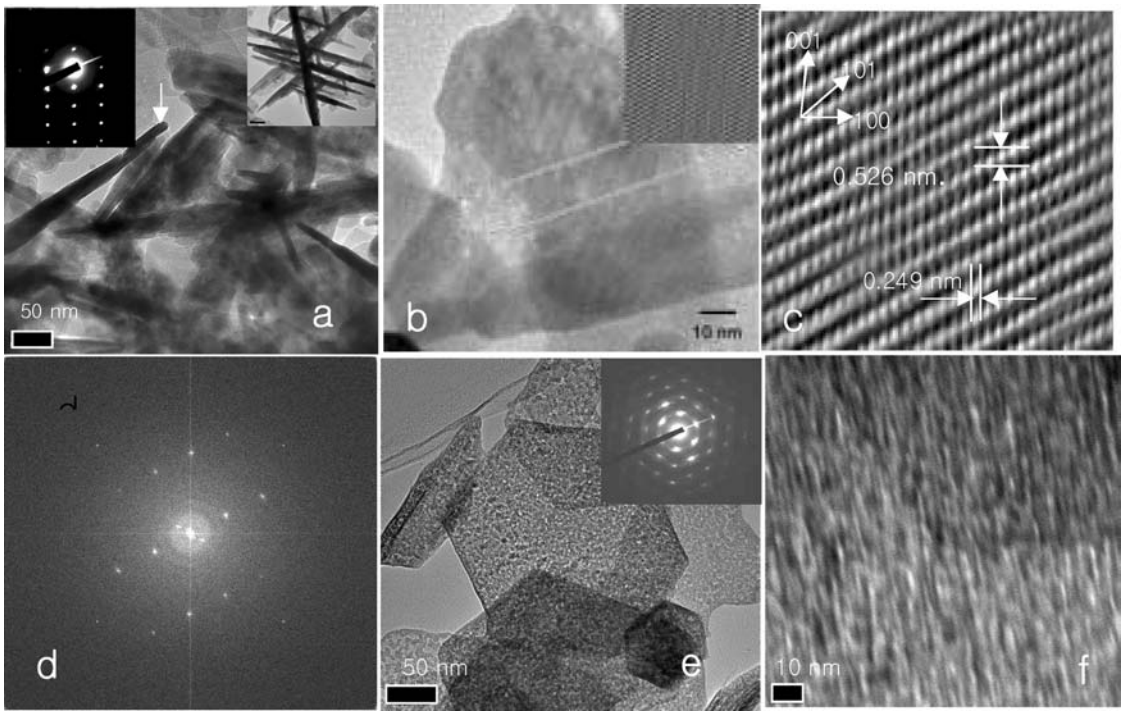

Figure 4 TEM analyses of the nanoslabs: (a) TEM image of single-crystalline ZnO bar-like nanoslabs; the right-hand inset displays nanoslabs having dendrite forms; the left-hand inset presents the SAED pattern recorded along the ⟨100⟩ zone axis (the arrow indicates the region of interest where the SAED pattern was recorded). (b) HRTEM image of single-crystalline nanoslabs recorded along the ⟨010⟩ zone axis; (c) a clearer magnified image of region marked in Fig. b; this image indicates oriented crystal growth along the [101] direction. (d) fast fourier transform (FFT) of the HRTEM region, which indicates crystal growth along the [101] direction. (e) TEM image of the polycrystalline nanoslabs; inset shows SAED pattern; the distinctive orientations indicate the polycrystalline nature. (f) HRTEM image of polycrystalline nanoslabs. The poor contrast of this image is due to the background signal from the amorphous carbon substrate.

Wurtzite structure. The result is also supported by Fast Fourier Transform (FFT) analysis of the HRTEM region, as depicted in Fig. 4d. We observe clearly from Fig. 4c that all the lattices are highly oriented along the *c*-axis. The lattice constant amount along the *c*-axis is 0.526 nm, as suggested by XRD. Simulating the XRD and TEM results, it may be proposed that the following three steps are involved for growing oriented ZnO nanoslabs [16]: first, formation of seeds (nuclei); second, the growth of random oriented crystals from the initial seeds; third, growth of nanoslabs oriented along ⟨101⟩ direction with continuous reaction for long time. It is noteworthy that the (002) reflection is much more intense than the (100) reflection in case of ZnO nanorod [16], nanobelt [13] or nanowire [21], whereas for the bulk ZnO, (002) reflection is comparatively less intense than the (100) reflection [22]. In our XRD pattern the intensity of (002) reflection is comparatively higher than the (100) reflections. Accordingly, it may be suggested that the growth direction continue along ⟨001⟩ direction even after ceasing the growth process along ⟨100⟩ and thus the growth maturity orient along ⟨101⟩ direction. No line defects or plane defects were observed in any of the examined areas. This finding does not mean, however, that other kinds of defects such as point defects, vacancies or interstitials, do not exist in the as-synthesized ZnO nanoslabs, because such defects may not be visible in the HRTEM images. Fig. 4e displays a TEM image of the polycrystalline nanoslabs. The SAED pattern recorded from the nanoslabs exposes two types of orientations (inset of Fig. 4e), indicating the existence of different crystallites, that are distincted from each other. The TEM image proves the physical existence of bi-crystalline phases ($Zn(OH)_2 \cdot 0.5H_2O$ and ZnO) (Fig. 4e), which shows that the nanoslabs are composed with white and black marks. Fig. 4f presents the HRTEM image of the polycrystalline product. The poor contrast of the image is due to the background signal from the amorphous carbon substrate [23] which may come from the lower specific gravity of the crystals.

However, the growth process of nanoslabs can simply be explained from a chemical point of view. In case of single crystal nanoslabs, when the NaOH concentration is high, selective adsorption of excess OH^- ions may be responsible either for oriented attachment of initially formed smaller clusters or face-selective addition of ions to the growing crystals. Similar case may happen with excess Zn^{2+} ions (at low NaOH concentration) for building up polycrystalline nanoslabs.

We systematically studied morphological features of our samples by changing various experimental parameters (temperatures, concentrations, stirring time, static condition time, and with and without implying the condensation-gradient technique). It was observed that all the parameters are strongly related to the nanoslab's architectures. For example, when the synthesis temperature was 25°C (without implying the condensation-gradient technique), spherical aggregated clusters were observed. That result suggests that the growth of random oriented crystals from the initial seeds is followed by subsequent aggregation due to the lack of sufficient temperature required for face-selective addition of ions to the growing crystals. On raising the oil bath temperature to 95°C (with implying the condensation-gradient technique), mixed clusters including irregular sheets were observed, plausibly due to the faster crystal growth at higher temperatures. When the static condition was not applied and the stirring time was less than 18 h, small clusters absorbed to the surface of the nanoslabs were observed. All the above results hint the superiority of the novel "condensation-gradient" method to control the stable morphology of the single crystalline and polycrystalline nanoslabs.

Thermogravimetric analysis (TGA) of polycrystalline nanoslabs (Fig. 5a) reveals that the weight loss up to 500°C is 27.5%, which is close to the theoretical weight loss (25%) after dehydration of ZnO from the $Zn(OH)_2 \cdot 0.5H_2O$ phase, whereas the weight loss of single-crystalline nanoslabs up to 500°C is 2.4% (Fig. 5b). The small degree of weight loss may arise from the endothermic effects due to molecular rearrangement upon recrystallization. In addition to the XRD results, EDS (data not shown) and TGA analyses of polycrystalline nanoslabs confirmed that the sample contains both $Zn(OH)_2 \cdot 0.5H_2O$ and ZnO phases. TGA results reveal that the nanoslabs are sufficiently stable within a working temperature range.

The optical properties of nanoslabs (at room temperature) are measured by UV-Vis absorption and photoluminescence spectroscopy with the identical molar concentration of suspensions. In Fig. 6a, spectrum *I* (single-crystal nanoslabs) shows the absorption maximum in the UV region at 382 nm. Usually, for wavelengths shorter than the absorption edge, scattering and absorption is effective, while for the longer wavelengths only scattering

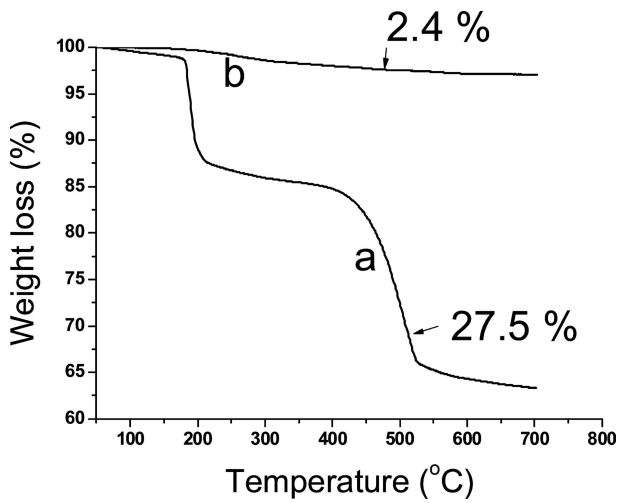

Figure 5 Thermogravimetric analyses of the nanoslabs. (a) TGA of polycrystalline nanoslabs. The weight loss up to 500°C is 27.5%, which is close to the theoretical weight loss (25.0%) that occurs after dehydration of the $Zn(OH)_2 \cdot 0.5H_2O$ phase to the ZnO phase. (b) TGA of the single-crystalline ZnO nanoslabs; the weight loss up to 500°C is 2.4%.

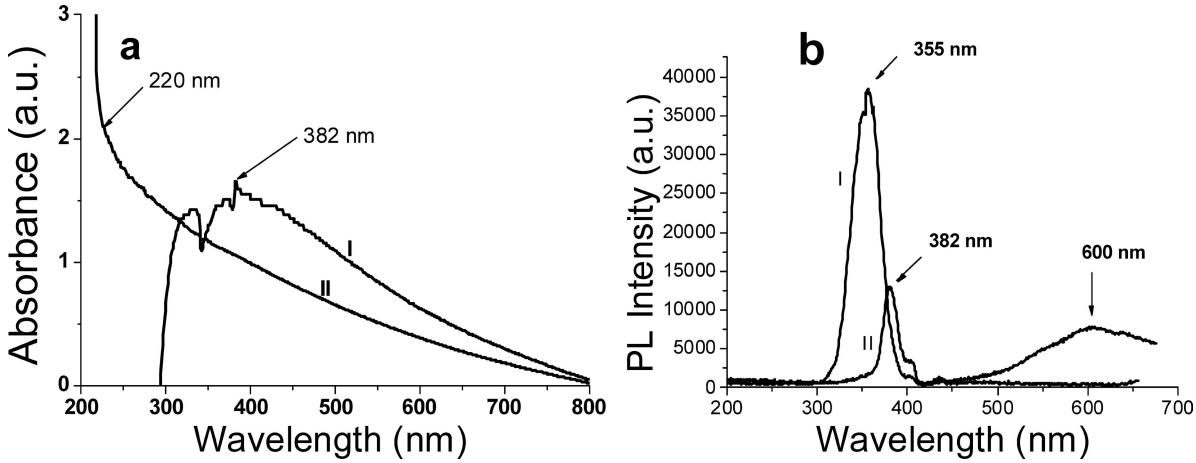

Figure 6 Room-temperature UV–Vis absorption and photoluminescence spectra: (a) (I) UV–Vis absorption spectrum of the single-crystalline ZnO nanoslabs; absorption maximum is located at 382 nm; (II) UV–Vis absorption spectrum of the polycrystalline nanoslabs; absorption maximum is shifted to 220 nm (band gap:~5.6 eV). (b) (I) Photoluminescence spectrum of the polycrystalline nanoslabs, exhibiting strong emission at ca. 355 nm. The emission energy in the UV range is ca. three-fold higher than the emission from the single-crystalline nanoslabs. (II) Photoluminescence spectrum of the single crystalline nanoslabs. The broad emission in the visible range occurs at ca. 600 nm; the emission in the UV range occurs at ca. 382 nm.

needs to be considered [24]. However, the absorption in the visible region should be generated only due to scattering, because larger particles have much higher scattering cross section [24] The absorption and corresponding band gap energy of bulk ZnO is $\lambda = 367$ nm and E_g=3.37 eV. The absorption band of single crystal nanoslabs was a little red-shifted from the absorption bands of wurtzite ZnO dendrities (377 nm) [25] and bulk ZnO (367 nm). The exact cause of the red -shift is not clear yet.

In case of polycrystalline nanoslabs, the absorption edge (indicated by arrow) has shifted to higher energy (band gap, E_g~5.60 eV), as shown in the spectrum II of Fig. 6a. 2.23 eV of blue shift was observed compared to the band gap of bulk ZnO (3.37 eV). This shifting should be due to the presence of the phase $Zn(OH)_2 \cdot 0.5H_2O$ in addition to the ZnO phase. The photoluminescence spectrum of polycrystalline nanoslabs (Fig. 6b, spectrum I) displays a potentially very useful phenomenon because the band gap energy is much higher than the exciton threshold energy of 3.4 eV (365 nm) and relatively large emission is observed at high energy UV region (3.5 eV) relative to the threshold value. This amplifying nature of the product is noteworthy.

Since we prepared the sample in Zn-rich condition, the excess Zn^{2+} ions in the materials reside on the surface, or at interfaces between the phases [26]. The small shift of emission relative to excitation threshold may be due to the interaction between the exciton and interface phonons [27]. The ultraviolet amplifying and photonic properties of those polycrystalline nanoslabs may be helpful for further applications such as laser emitters, storage devices and fluorescence markers.

The PL spectrum of the single-crystalline nanoslabs (spectrum II, Fig. 6b), however, showed a strong and sharp emission band centered at 382 nm displays within the UV range and a countable broad emission peak centered at ~600 nm in the visible region, when the same excitonic photon energy (3.4 eV) was applied. These two emission peaks are well consistent with the previously reported articles [1, 10, 28]. The emission peak, 600 nm, may come from the recombination of a photogenerated hole with a singly ionized charge state of the specific defect due to the singly ionized oxygen vacancy [1, 29–30].

In addition, single-crystalline nanoslabs possess strong and selective chemical sensitivity when 4-triethoxysilylaniline was added to an aqueous suspension of the as synthesized ZnO single crystals (in a sealed state at 45°C); their white color changed to dark brown (Fig. 7), but no color change occurred when 3-triethoxysilylpropylamine was added. This finding suggests that the single-crystalline ZnO nanoslabs can be used in devices for selective chemical sensing. The adsorption of 4-triethoxysilylaniline may, however, promote

Figure 7 Chemical sensing by the single-crystalline nanoslabs: (a) ampoule containing a colloidal suspension of single-crystalline ZnO, which appears white; (b) the appearance of the ampoule (deep-brown suspension) after the addition of 4-triethoxysilylaniline (sample taken after 4 h of addition) and (c) the appearance of the ampoule (dark-brown solution) after sedimentation. (d) The appearance of the ampoule (white suspension) after the addition of 3-ethoxysilylpropylamine (sample taken after 4 h of addition) and (e) the appearance of the ampoule (semi-opaque white solution) after sedimentation.

coloration because of formation of charge transfer complexes with surface Zn cations. The aromatic compounds with electron-donating group (NH_2) promote color formation [31].

4. Conclusions

In summary, single-crystal and polycrystal nanoslabs could be obtained by a one-step synthesis using a "sol-gel-via-condensation-gradient" method without using any surfactant or stabilizing agent. Producing nanocrystals this way is cheap and facile, but it results in materials that have high optical quality. With a well-defined shape and perfect crystallinity, the nanoslabs are likely to be a model material's family for a systematic experimental and theoretical understanding in the fundamental electrical, thermal, optical and ionic transport processes.

Acknowledgements

This work was supported by the National Research Laboratory Program, the Center for Integrated Molecular Systems and Brain Korea 21 Project.

References

1. J. Q. HU and Y. BANDO, *App. Phys. Lett.* **9** (2003) 1401.
2. W. I. PARK, Y. H. JUN, S. W. JUNG and G. C.YI, *ibid.* **82** (2003) 964.
3. L. GUE, Y. L. JI and H. XU, *J. Am. Chem. Soc.* **124** (2002) 14864.
4. G. GORDILLO, *Surf. Rev.Lett.* **9** (2002) 1675.
5. B. O'REGAN and M. GRATZEL, *Nature* **353** (1991) 737.
6. H. L. HARTNAGNEL, A. L. DAWAR, A. K. JAIN and C. JAGIDISH, "Semiconducting transparent thin films", Institute of Physics publishing, Philadelphia, PA (1995).
7. B. PAL and M. SHARON, *Mater. Chem. Phys.* **76** (2002) 82.
8. F. K. CHIVIROVA, A. K. AVETISOV, S. A. KAZAKOV, L. A. OBVINTSEVA and M. V. STROBKOVA, *Sensors.* **3** (2003) 451.
9. Y. CUI, Q. WEI, H. PARK and C. M. LIEBER, *Science.* **293** (2001) 1289.
10. Y. C. KONG, D. P. YU, W. FANG, B. ZHANG and S. Q. FENG, *App. Phys. Lett.* **78** (2001) 407.
11. L. VAYSSIERS, *Adv. Mater.* **15** (2003) 464.
12. W. I. PARK, G.-C. YI, M. KIM and S. J. PENNYCOOK, *ibid.* **14** (2002) 1841.
13. Z. W. PAN, Z. R. DAI and Z. L. WANG, *Science.* **291** (2001) 1947.
14. H. YAN, R. HE, J. PHANS and P. YANG, *Adv. Mater.* **15** (2003) 402.
15. J. HU, Y. BANDON and Z. LIU, *ibid.* **15** (2003) 100.
16. Z. R. TIAN, J. A. VOIGT, J. LIU, B. MCKENZIE, M. J. MCDERMOTT, M. A. RODRIGUEZ, H. KONISHI and H. XU, *Nature Materials.* **2** (2003) 821.
17. C. LOPEZ, *Adv. Mater.* **15** (2003) 1679.
18. L. SANHEL and M. A. ANDERSON, *J. Am. Chem. Soc.* **113** (1991) 2826.
19. L. N. DEMINANTS, D. V. KOSTOMAROV, I. P. KUZIMINA and S. V. KPUSHKO, *Crystallography Reports.* **47** (2003) s86.
20. K. SUE, K. MURATA, K. KIMURA and K. ARAI, *Green Chem.* **5** (2003) 659.
21. M. H. HUANG, Y. WU, H. FEICK, N. TRAN, E. WEBER and P. YANG, *Adv. Mater.* **13** (2001) 113.
22. X. ZHONG and W. KNOLL, *Chem. Commun.* (2005) 1158.
23. P. REISS, J. BLEUSE and A. PRON, *Nano Lett.* **2** (2002) 781.
24. S. M. SCHOLZ, R. VACASSY, J. DUTTA and H. HOFMANN, *J. Appl. Phys.* **83** (1998) 7860.
25. S. H. YU, J. YANG, Y. T. QIAN and M. YOSHIMURA, *Chem. Phys. Lett.* **361** (2002) 362.
26. K. MEHRANY, S. KHORASANI and B. RASHIDIAN, *Semicond. Sci. Technol.* **18** (2003) 1.
27. W. CHEN, J. Z. ZHANG and A. G. JOLY, *J. Nanosci. Nanotech.* **4** (2004) 919.
28. X. WANG, C. J. SUMMERS and Z. L. WANG, *Nano Lett.* **4** (2004) 423.
29. D. BANERJEE, J. Y. LAO, D. Z. WANG, J. Y. HUANG, Z. F. REN, D. STEEVES, B. KIMBALL and M. SENNETT, *App. Phys. Lett.* **83** (2003) 2061.
30. L. E. GREENE, M. LAW, J. GOLDBERGER, F. KIM, J. C. JHONSON, Y. R. J. SAYKALLY and P. YANG, *Angew. Chem. Int. Ed..* **42** (2003) 3031.
31. N. C. SHANH and Y. H. YU, *Environ. Technol.* **23** (2002) 43.

Received 24 March 2005
and accepted 11 July 2005